*Desalination and Water Treatment*
www.deswater.com

doi: 10.5004/dwt.2017.21407

100 (2017) 135–144
December

# Equilibrium, kinetics, and thermodynamics studies of Cr(VI) adsorption from aqueous solutions on organoclay using ionic liquid-type imidazolium surfactants

Yaqin Liang*, Yan Li*, Shuping Zhang, Hui Li, Xiaoming Mao, Lihua Zhou, Wenzhuo Yang

*Department of Chemistry, Changzhi College, Changzhi, Shanxi 046000, China, Tel. 86-0355-2178113, Fax 86-0355-2178113, email: liangyaqinfaye@126.com (Y. Liang), liyan_china@126.com (Y. Li), 13903552986@139.com (S. Zhang), 109973381@qq.com (H. Li), 21806793@qq.com (X. Mao), 378036414@qq.com (L. Zhou), 13903550865@139.com (W. Yang)*

Received 26 April 2017; Accepted 26 November 2017

**ABSTRACT**

The organoclays $C_{12}$ mim Br-Mt and $C_{16}$ mim Br-Mt were prepared using the ionic liquid-type imidazolium surfactants 1-dodecyl-3-methylimidazolium bromide ($C_{12}$ mim Br) and 1-hexadecyl-3-methyl-imidazolium bromide ($C_{16}$ mim Br) with sodium montmorillonite (Na-Mt). Then, $C_{12}$ mim Br-Mt and $C_{16}$ mim Br-Mt were characterized using X-ray diffraction (XRD), fourier transform infrared (FTIR) spectroscopy, thermogravimetric analysis (TG), and scanning electron microscopy (SEM). The results showed that $C_{12}$ mim Br and $C_{16}$ mim Br were successfully inserted into the lamella of Na-Mt, and the interlayer spacing was related to the alkyl chain length and the loading level of the surfactants. The adsorption of Cr (VI) on $C_{12}$ mim Br-Mt and $C_{16}$ mim Br-Mt was studied using the operational variables, including the loading level of the surfactants, contact time, and pH. The optimal conditions were as follows: the loading level of surfactants up to two times of cation exchange capacity (CEC) of Na-Mt, contact time of 2.0 h, and pH of 2.0. At the same experimental conditions, $C_{16}$ mim Br-Mt had stronger affinity for negatively charged Cr(VI) because of electrostatic interactions. The equilibrium adsorption data showed that the adsorption of Cr(VI) on organoclay correlated well with the Langmuir isotherm model. Using this model, the maximum adsorption capacities were 20.97 $mg \cdot g^{-1}$ and 24.56 $mg \cdot g^{-1}$ for $C_{12}$ mim Br-Mt and $C_{16}$ mim Br-Mt, respectively. The kinetics study indicated that the adsorption of Cr(VI) onto $C_{12}$ mim Br-Mt and $C_{16}$ mim Br-Mt followed a pseudo-second order model. The thermodynamics parameters, $\Delta G^{\theta}$, $\Delta H^{\theta}$, and $\Delta S^{\theta}$, were calculated, and the results indicated that the adsorption of Cr (VI) onto organoclay was an exothermic spontaneous physisorption process.

*Keywords:* Adsorption; Ionic liquid surfactant; Isotherms; Kinetics

## 1. Introduction

As industrialization and urbanization have developed, a considerable amount of industrial effluents have been emitted, and water quality continues to deteriorate. Heavy metals are one of the most problematic pollutants because of their persistent, non degradable, and accumulative nature [1,2]. Chromium is one of the most notorious heavy metals released by various industries such as leather tanning, textile dying, metal finishing, electroplating, ceramics, and glass manufacturing [3,4]. Hexavalent chromium Cr(VI) is a highly toxic and soluble form of the element chromium. Much of the Cr(VI) may be in the form of dichromate ($Cr_2O_7^{2-}$), hydrochromate ($HCrO_4^-$), and chromate ($CrO_4^{2-}$), and these are dangerous to human beings and the environment because of their mutagenicity and carcinogenic properties. Additionally, they can cause internal hemorrhaging, nausea, diarrhea, and liver and kidney damage [5]. Numerous efforts have been made to minimize the impact of Cr(VI) by using electro coagulation, cation exchange, chemical precipitation, membranes, and adsorption over solid adsorbents [6–11]. Of these efforts, adsorption technology is widely used in industry because of its simple design, low-cost, high effectiveness, possible reuse of the adsorbents, and facile handling process [12,13].

*Corresponding author.

Montmorillonite (Mt) is a typical 2:1 type clay mineral and has been reported to be a good adsorbent because of its special layered structures, abundance in nature, low cost, and ion exchange capacity [14]. However, it has little affinity for anionic groups. Thus, different methods have been introduced to modify Mt, including acid activation, physical coating, and organic quaternary ammonium salts [4,15–18]. In fact, modifications with cationic surfactants have rapidly become important because cationic surfactants change the surface characteristics of Mt, and this makes modified Mt favorable for the adsorption of Cr(VI). Akar et al. reported that the Cr(VI) adsorption capacity of hexadecyltrimethyl ammonium-modified Mt increased to 10.18 mg·g$^{-1}$, which is nearly 2.8 times greater than natural Mt [17]; Kumar et al. found that 23.69 mg·g$^{-1}$ Cr(VI) adsorption can be achieved using dodecylamine-modified Mt [18]. Wang et al. found that the Cr(VI) adsorption capacity of dodecyltrimethyl ammonium chloride-modified Mt was 10.44 mg·g$^{-1}$, according to a pseudo-second order reaction kinetics model [19]. Luo et al. reported that the maximum adsorption capacity of Cr(VI) onto Mt modified with hydroxy aluminum and cetyltrimethyl ammonium bromide was 11.97 mg·g$^{-1}$ [20]. Ionic liquid-type imidazolium surfactants (ILIs), such as 1-alkyl-3-methyl-imidazolium salts, have characteristics of both ionic liquids and surfactants. Compared to conventional quaternary ammonium surfactants, the imidazolium-based surfactants have special qualities; for example, they are environmentally friendly compounds, more thermally stable, self aggregate more strongly. They have lower critical micelle concentration (CMC) and novel surface properties, all of which result from the delocalized positive charge on the imidazolium ring and the ubiquitous hydrogen bonds among the imidazolium cations [21–23]. Urahata used molecular simulations and showed that positions above and below the imidazolium ring are preferential positions for large anions [24]. Combined with the above information, ILI shave emerged as a kind of intercalating agent to synthesize the organo-montmorillonites (OMts).

The purposes of this study were to synthesize the $C_{12}$mim-Br-Mt and $C_{16}$ mim Br-Mt modified with the imidazolium cationic surfactants, 1-dodecyl-3-methyl-imidazoliumbromide ($C_{12}$ mim Br) and 1-hexadecyl-3-methyl-imidazolium bromide ($C_{16}$ mim Br). The structures of the OMts were characterized using X-ray diffraction (XRD), Fourier transform infrared (FTIR) spectroscopy, and thermogravimetric analysis (TG). Additionally, batch adsorption experiments were conducted to investigate the effects of loading level of surfactants, contact time, and pH on the adsorption behavior of Cr(VI) on OMts. The adsorption model and adsorption thermodynamics are discussed to further assess the adsorption capacity and to explore the adsorption mechanism of OMts. The findings of this study provide an experimental basis for the design and fabrication of highly effective OMts as adsorbents to remove Cr(VI) from wastewater.

## 2. Methods and apparatus

### 2.1. Materials

1-dodecylbromide, 1-hexadecylbromide, and N-methylimidazole were purchased from Aldrich Chemical Co., Ltd. Na-Mt with a cation exchange capacity (CEC) of 90 meq·100 g$^{-1}$ was procured from Zhejiang Fenghong New Materials Co., Ltd. Diphenyl carbazide was purchased from Tianjin Damao Chemical Reagent Co., Ltd., and was analytical grade. Potassium dichromate ($K_2Cr_2O_7$), acetone, and acetonitrile were analytical grade and were provided by Beijing Institute Reagent Co., Ltd. The pH of the aqueous solution was regulated using HCl and NaOH (0.1 mol·L$^{-1}$). The water used in all of the experiments was triple-distilled water.

### 2.2. Preparation of $C_{12}$mim Br and $C_{16}$mim Br

The chemical structures of $C_{12}$ mim Br and $C_{16}$ mim Br are shown in Fig. 1. $C_{12}$ mim Br and $C_{16}$ mim Br were synthesized according to a procedure described by Rahmat in previous publications [23,25]. 1-bromoalkane (1.1 mol equiv) was added to 50 mL of the acetonitrile solution of N-alkylimidazole (1.0 mol equiv). The mixture was heated under are flux condenser for 12.0 h and stirred constantly. Free 1-bromoalkane was extracted several times using hexane. A brown oily or gelatinous product was obtained via vacuum distillation of the solution. The white products obtained were recrystallized three times from acetone and dried under vacuum. $C_{12}$ mim Br: yield: 92%; $^1$H NMR (400 MHz, $CDCl_3$): δ 0.82 (t, 3H). 1.22–1.34 (m, 18H), 1.82–2.19 (m, 2H), 4.10 (s, 3H), 4.26 (t, 2H), 7.39 (d, 1H), 7.58 (d, 1H), 10.18 (s, 1H). Analysis calculated for $C_{16}H_{31}BrN_2$: C, 58.00; H, 9.43; N, 8.45. Found: C, 58.34; H, 9.49; N, 8.87. $C_{16}$ mim Br: yield: 95%; $^1$H NMR (400 MHz, $CDCl_3$): δ 0.84 (t, 3H). 1.19–1.32 (m, 24H), 1.87–2.16 (m, 4H), 4.11 (s, 3H), 4.31 (t, 2H), 7.43 (d, 1H), 7.65 (d, 1H), 10.22 (s, 1H). Analysis calculated for $C_{20}H_{39}BrN_2$: C, 62.00; H, 10.15; N, 7.23. Found: C, 62.45; H, 10.23; N, 7.06. The data was inconsistent with the literature [24].

### 2.3. Preparation of $C_{12}$min Br-Mt and $C_{16}$min Br-Mt

OMts were prepared using a simple ion exchange method. Typically, 5.0 g of Na-Mt was dispersed in 250 mL of deionized water at 60°C for 1 h. Amounts of $C_{12}$ mim Br or $C_{16}$ mim Br (equivalent to 0.4, 0.8, 1.0, 1.5, 2.0, or 3.0 times that of the CEC of Na-Mt) were dissolved in 250 mL of deionized water. The $C_{12}$ mim Br or $C_{16}$ mim Br solution was then slowly added to the Na-Mt suspension. The mixture was vigorously stirred for 3.0 h at 80°C. Afterward, the solid was separated by centrifugation and washed several times with triple-distilled water until the wash water was free of bromide ions (tested using 0.1 mol·L$^{-1}$ $AgNO_3$). After filtration, the OMts were dried, ground, sieved, and named $C_{12}$ min Br-Mt and $C_{16}$ min Br-Mt, respectively.

### 2.4. Characteristic analysis

FTIR spectra were recorded using a NICOLET 380 spectrometer (Thermo Nicolet Co.,USA) in the wave number

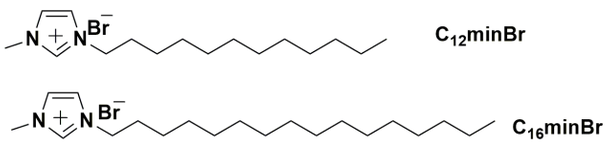


Fig. 1. Chemical structures of $C_{12}$ mim Br and $C_{16}$ mim Br.

range of 400–4000 $cm^{-1}$ at a resolution of 4 $cm^{-1}$. $^1H$ nuclear magnetic resonance (NMR) spectra were recorded using a Bruker Avance NMR spectrometer (Model ARX-400, Bruker Bio Spin Co., Switzerland) using tetramethylsilane as the internal standard. Elemental analyses were measured using an elemental analyzer (Model Vario EL, Elementar Analysensysteme GmbH, Germany). XRD patterns of the samples were recorded using an XRD-6100 X-ray diffraction (Shimadzu Ltd., Japan) operating at 40 kV and 40 mA using a monochromator with a Cu/Kα radiation (incident angle = 0.5°, λ = 1.541Å, step size = 0.5°, integration time 20 s·step$^{-1}$). The thermal stability of the samples was measured on a thermogravi metric analyzer (Model STA 449 F1, NETZSCH Scientific Instruments Trading Ltd., Germany). The temperature ramps were from 20 to 800°C with a heating rate of 10°C·min$^{-1}$ under a nitrogen environment. The morphological studies were carried out using a scanning electron microscope (JSM-2100, Electron Optics Co., Japan). UV spectra were recorded using a UV-Vis spectrophotometer (U-2910, Hitachi Co., Japan).

### 2.5. Adsorption experiments

The adsorption of Cr (VI) on $C_{12}$ mim Br-Mt and $C_{16}$ mim Br-Mt was conducted using a batch adsorption method based on operational variables, including the loading level of the surfactants, contact time, and pH. The stock solution of Cr (VI) was prepared by dissolving 0.1414 g of $K_2Cr_2O_7$ in triple-distilled water and diluting to 100 mL. In all of the batch adsorption studies, solutions of 25–200 mg·L$^{-1}$ concentrations were used. To determine the effects of loading level of surfactants, 100 mg of $C_{12}$ min Br-Mt or $C_{16}$ min Br-Mt (0.2–3.0 CEC) was dispersed in 250 mL conical flasks containing 50 mL of 50 mg·L$^{-1}$ Cr (VI) with an initial pH value of 6.7. The experiments were carried out at 20°C using water incubator shakers with a speed of 200 rpm for 4.0 h, which was determined by preliminary tests. After centrifugation, the concentration of the residual Cr(VI) was analyzed using UV-vis spectroscopy at $\lambda_{max}$ 540 nm. The percent (%) removal of Cr(VI) and the adsorption amount of Cr (VI) on OMts were calculated using Eqs. (1) and (2), respectively

$$R = \frac{C_i - C_e}{C_i} \times 100\% \quad (1)$$

$$q_e = \frac{(C_i - C_e) \times V}{m} \quad (2)$$

where $C_i$ and $C_e$ are the initial and equilibrium concentrations, respectively, of Cr (VI) (mg·L$^{-1}$). $R$ is the removal efficiency of Cr(VI) on OMts, and $q_e$ (mg·g$^{-1}$) is the adsorption amount of Cr (VI) on OMts at various times. $V$ (L) is the solution volume, and $m$ (g) is the mass of $C_{12}$ min Br-Mt or $C_{16}$ min Br-Mt.

To determine the effects of the solution pH on Cr(VI) adsorption, experiments were carried out by adjusting the initial solution pH to 2.0, 4.0, 6.0, 6.7, 9.0, and 11.0 with the addition of 0.1 mol·L$^{-1}$ HCl or 0.1 mol·L$^{-1}$ NaOH solution. The effects of the contact time were assessed within 4.0 h at different intervals with an initial Cr (VI) concentration of 50 mg·L$^{-1}$. Adsorption isotherms were obtained at 20°C by mixing 100 mg of Na-Mt, $C_{12}$ min Br-Mt, or $C_{16}$ min Br-Mt with 50 mL of Cr (VI) solution with various concentrations that ranged from 25 mg·L$^{-1}$ to 200 mg·L$^{-1}$.

## 3. Results and discussions

### 3.1. Characterization of $C_{12}$ min Br-Mt and $C_{16}$ min Br-Mt

The infrared spectra of $C_{12}$ min Br-Mt and $C_{16}$ min Br-Mt were presented in Figs. 2a and b, respectively. The characteristic band of Na-Mt, $C_{12}$ min Br-Mt, and $C_{16}$ min Br-Mt at 3640–3400 $cm^{-1}$ was attributed to the stretching vibrations of Al–O–H and H–O–H, which may arise from the isomorphic substitution in the tetrahedral and octahedral layers of Mt [27]. The band at 1640 $cm^{-1}$ corresponded to the bending vibration of physisorbed water. After intercalating Na-Mt with $C_{12}$ min Br-Mt or $C_{16}$ min Br-Mt, two new distinct adsorption peaks at 2925 $cm^{-1}$ and 2845 $cm^{-1}$ were observed,

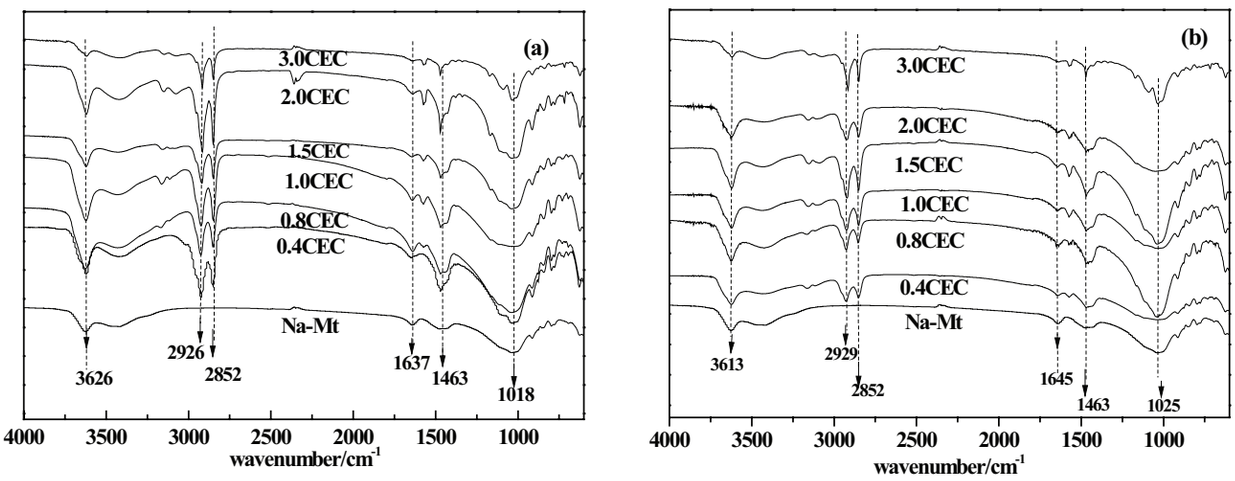


Fig. 2. FTIR spectra of $C_{12}$ min Br-Mt (a) and $C_{16}$ min Br-Mt (b).

and these were assigned to the asymmetric and symmetric stretching vibrations of C–H in methyl groups, respectively. The band at 1472 $cm^{-1}$ was assigned to the bending vibration of the C–H bonds in $C_{12}$ min Br-Mt and $C_{16}$ min Br-Mt. It can be concluded that $C_{12}$ min Br or $C_{16}$ min Br were successfully intercalated into Na-Mt via an ion-exchange interaction.

Figs. 3a and b show the XRD patterns of $C_{12}$ min Br-Mt and $C_{16}$ min Br-Mt, respectively, with different surfactant loading. The XRD pattern of Na-Mt had a peak at 2θ = 6.72, and this was assigned to the [001] reflection; the corresponding basal spacing $d_{001}$ was 1.31 nm according to the Bragg equation, λ = 2 d sinθ, and this corresponded to a thickness of one Mt layer (0.97 nm) plus the distance of the hydrated sodium-bearing interlayer [27]. In Fig. 3a, the 2θ values shifted to 5.03°, 4.94°, 4.50°, 4.38°, 4.32°, and 4.02° as the amount of $C_{12}$ min Br loading was increased to 0.4, 0.8, 1.0, 1.5, 2.0, and 3.0 CEC, respectively, and the $d_{001}$ values were 1.74, 1.79, 1.96, 2.02, 2.05, and 2.21 nm, respectively. As shown in Fig. 3b, the 2θ values shifted to 5.46°, 4.25°, 4.02°, 3.98°, 3.77°, and 3.27° as the amount of $C_{16}$ min Br was increased to 0.4, 0.8, 1.0, 1.5, 2.0, and 3.0 CEC, respectively, and the $d_{001}$ values were 1.62, 2.08, 2.20, 2.22, 2.34, and 2.70 nm, respectively. This showed that $C_{12}$ min Br or $C_{16}$ min Br were intercalated into the interlayer of Na-Mt, the $C_{12}$ min Br or $C_{16}$ min Br monomers were retained via ion exchange and eventually formed monolayers for OMts at lower loading levels. For OMts at higher loading levels, interactions among the hydrocarbon tails caused bilayers to form, leading to an obvious increase in the interlayer distance of Na-Mt [25]. With an increase in the length of the hydrocarbon chain, either $C_{16}$ min Br-Mt benefited from having a larger inter lamellar spacing, or $C_{16}$ min Br was more efficient at enlarging the basal spacing of Na-Mt than $C_{12}$ min Br.

The thermogravimetric analyses and derivative thermogravimetric curves (TG-DTG) were obtained to examine the influence of ILIs inserted layer of Na-Mt on the thermal behavior. The TG-DTG thermo grams of Na-Mt, $C_{12}$ min Br-Mt (2.0 CEC), and $C_{16}$ min Br-Mt (2.0 CEC) are shown in Figs. 4a and 4b, respectively. An 8.41% weight-loss was observed in the temperature range of 20–200°C, and a 6.89% weight-loss appeared at 350–800°C. The first occurred because of the dehydration of physically adsorbed water and water molecules around $Na^+$ on exchangeable sites in Mt [26]. The second was related to the structural water released when one alumina octahedral sheet was sandwiched between two silica tetrahedral sheets [27]. It should be noted that the broad and weak bands around 666.56°C

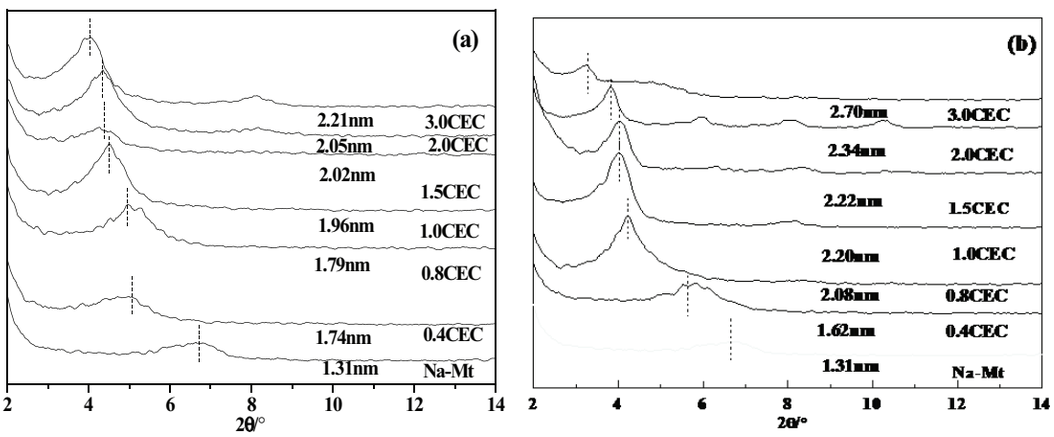


Fig. 3. XRD patterns of $C_{12}$ min Br-Mt (a) and $C_{16}$ min Br-Mt (b).

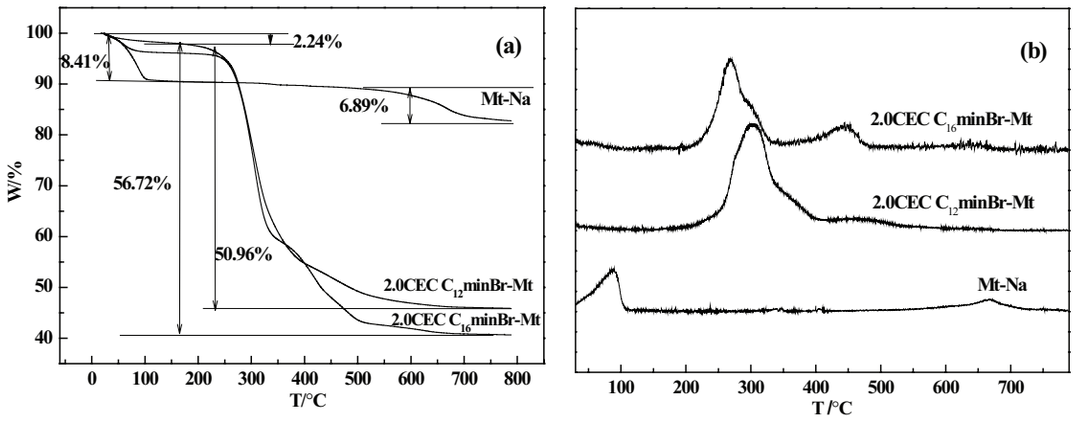


Fig. 4. TG (a) and DTG (b) curves of Na-Mt, $C_{12}$ min Br-Mt, and $C_{16}$ min Br-Mt.

in the DTG curve can be assigned to the structural water released during the dehydroxylation/dehydration processes [28]. For $C_{12}$ min Br-Mt (2.0 CEC) and $C_{16}$ min Br-Mt (2.0 CEC), it can be observed that a 2.24% weight-loss was assessed in the temperature range of 20–100°C; this weight-loss was smaller than that of Mt-Na, which suggested that $C_{12}$ min Br-Mt (2.0 CEC) and $C_{16}$ min Br-Mt (2.0 CEC) could reduce the surface energy of Mt-Na and change the hydrophilic surface property to hydrophobic because of the substitution of hydrated $Na^+$ by $C_{12}$ min Br or $C_{16}$ min Br. This result agreed with the results obtained from the FTIR spectra. Between 200 and 800°C, weight-losses of 50.96% for $C_{12}$ min Br-Mt and 56.72% for $C_{16}$ min Br-Mt were much larger than that for Mt-Na (6.89%), and this was because of the dehydration of the crystal lattice and the decomposition of carbon residues from the ILIs [28].

As shown in Fig. 4b, the evaporation and decomposition of $C_{12}$ min Br-Mt occurred at 307.26 and 479.55**°C**, respectively, and at 267.56 and 446.37**°C**, respectively, for $C_{16}$min-Br-Mt. The peaks at higher temperatures were attributed to combustion and to the loss of pure and intercalated surfactant molecules. These results confirmed that the intercalating surfactants affected the thermal stability of the OMts. In contrast, the thermal stability decreased as the organic content of the molecule increased.

The morphological characteristics of Na-Mt, 2.0 CEC $C_{12}$ mim Br-Mt, and 2.0 CEC $C_{16}$ mim Br-Mt were evaluated using scanning electron microscopy (SEM), and the micrographs are given in Figs. 5a–c. Fig. 5a shows that large numbers of tabulate plates were visible in Na-Mt. In contrast, $C_{12}$ mim Br-Mt and $C_{16}$ mim Br-Mt (Figs. 5b and c) had curled and crumpled morphologies. The changes in the surface morphology occurred as particles agglomerated. The observed structural changes positively affected the adsorption properties of $C_{12}$ mim Br-Mt and $C_{16}$ mim Br-Mt.

### 3.2. Batch adsorption

The experiments were done for loading levels of 0.4, 0.8, 1.0, 1.5, 2.0, and 3.0, an adsorbent dose of 2.0 $g \cdot L^{-1}$, an initial concentration of 50 $mg \cdot L^{-1}$, contact time of 4.0 h, and pH of 6.7 at room temperature. Fig. 6 depicts the loading level of the surfactants on the efficiency of Cr(VI) removal (R) by $C_{12}$ min Br-Mt and $C_{16}$ min Br-Mt. Compared to Na-Mt (the value of R did not exceed 0.53%), the use of OMts for Cr(VI) adsorption was more favorable. When the loading level of the surfactants increased to 0.4 CEC, the value of R slowly increased to 4.04 % for $C_{12}$ min Br-Mt and 1.68% for $C_{16}$ min Br-Mt. When the loading level of the surfactants exceeded 0.4 CEC, the value of R increased to 78.19 % for 2.0 CEC $C_{12}$ min Br-Mt and to 90.14% for 2.0 CEC $C_{16}$ min Br-Mt; the value of R increased to 83.76% for 3.0 CEC $C_{12}$ min Br-Mt and to 94.25% for 3.0 CEC $C_{16}$ min Br-Mt. Clearly, a relatively high loading level of $C_{12}$ min Br-Mt or $C_{16}$ min Br-Mt was necessary. According to the XRD results, the configuration of imidazolium surfactants might change from monolayers to bilayers into interstitial layers with the loading level of surfactants from 0.4 CEC to 3.0 CEC [29]. The increased surfactant loading led to a higher packing density of surfactants per unit basal area and highly ordered chain arrangements; consequently, the positively charged imidazolium head group had stronger affinity for the negatively charged Cr(VI) because of the electrostatic interaction. Considering the value of R and the price of ILIs, 2.0 CEC of $C_{12}$ min Br-Mt and 2.0 CEC of $C_{16}$ min Br-Mt were chosen as representative samples to study in the adsorption experiments.

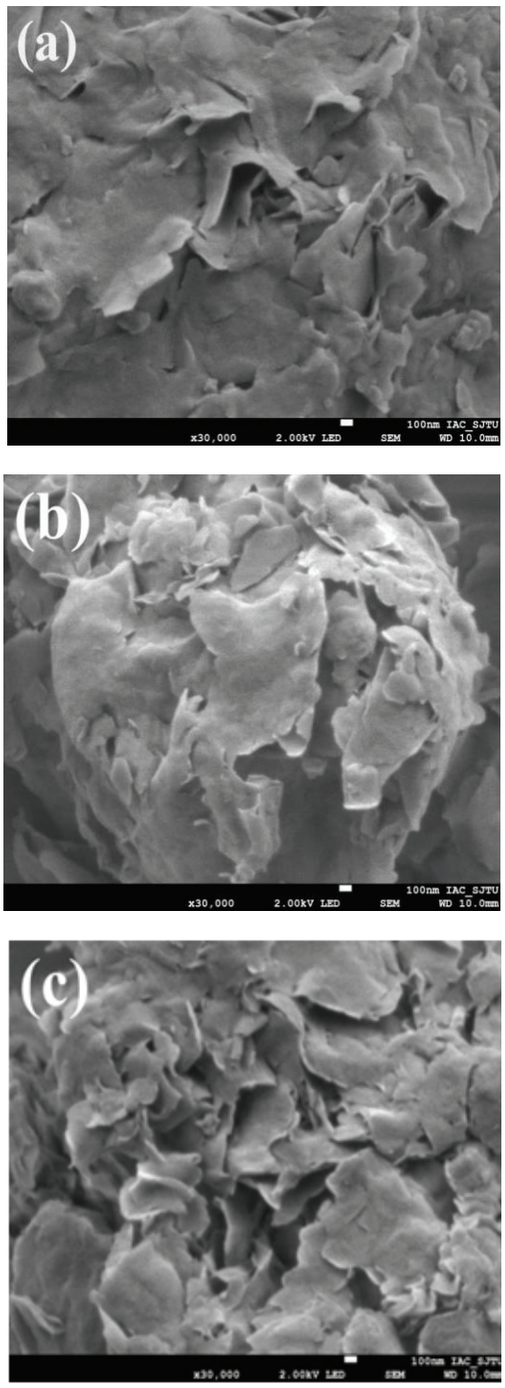


Fig. 5. SEM micrographs of Na-Mt (a), 2.0 CEC $C_{12}$ mim Br-Mt (b), and 2.0 CEC $C_{16}$ mim Br-Mt (c).

In addition, the value of R for $C_{16}$ min Br-Mt was higher than that for $C_{12}$ min Br-Mt at the same loading level. The roles that the length of the hydrophobic chain played in

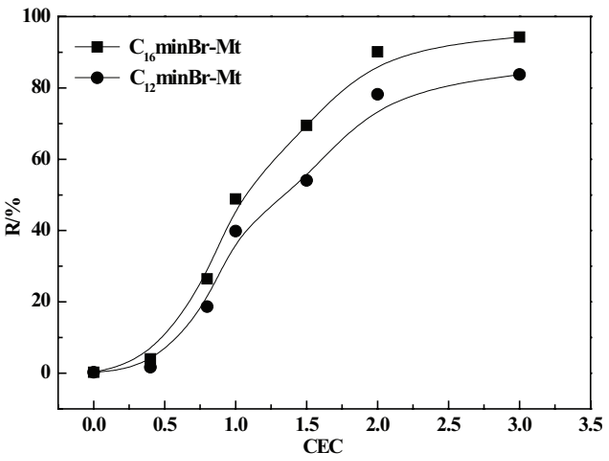


Fig. 6. Effects of the loading level on the efficiency of Cr(VI) removal using $C_{12}$ min Br-Mt and $C_{16}$ min Br-Mt.

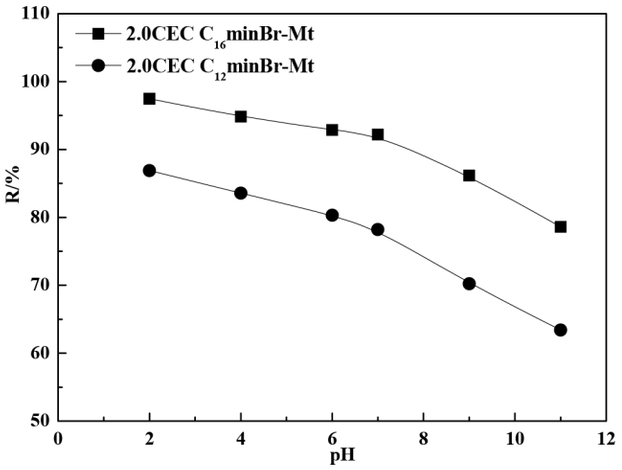


Fig. 7. Effects of pH on the efficiency of Cr(VI) removal using $C_{12}$ min Br-Mt and $C_{16}$ min Br-Mt.

forming the sorbed surfactant bilayers can be compared to the roles they played in forming micelles in solution. First, the length of the hydrophobic chain affected the CMC. Specifically, the longer that the hydrophobic chain of the cationic surfactant was, the lower that the value of the CMC was; the smaller that the ratio between the monomers and micelles at a given solution concentration was, the higher that the likelihood of monomers associating to form micelles in solution or to form admicelles on the surface was. Therefore, it may be concluded that the ratio of the bilayer to monolayer for $C_{16}$ min Br-Mt was larger than that for $C_{12}$ min Br-Mt. This also confirmed that $C_{16}$ min Br-Mt had a higher packing density of surfactants per unit basal area than $C_{12}$ min Br-Mt had at the same loading level. Thus, the value of R for $C_{16}$ min Br-Mt was higher. Second, the increased surfactant loading caused the length of the hydrophobic chain to affect the aggregation number and thus the size of the micelles. Li reported that $C_{12}$ min Br and $C_{16}$ min Br can form micelles in aqueous solution, and the mean aggregation numbers of $C_{12}$ min Br and $C_{16}$ min Br in aqueous solutions at 25°C were 44–67 and 66–114, respectively [30]. The micelles of $C_{16}$ min Br had obviously bigger aggregation numbers and bigger micellar hydrodynamic radius. Similarly, the sorption density of the second layers for $C_{16}$ min Br was higher when ILIs were sorbed onto the surface of the Na-Mt, which resulted in more bilayer coverage and higher values of R.

pH was a major factor that affected the adsorption process. The experiments in the pH range of 2.0–11.0 were done with an adsorbent dose of 2.0 CEC, 2.0 g·L$^{-1}$, an initial concentration of 50 mg·L$^{-1}$, and contact time of 4.0 h. Fig. 7 showed the effects of pH on the efficiency of Cr(VI) removal (R) using $C_{12}$ min Br-Mt and $C_{16}$ min Br-Mt. The value of R increased with the value of pH from 11.0 to 2.0, and the value of R increased to 86.97% and 96.47% for $C_{12}$ min Br-Mt and $C_{16}$ min Br-Mt, respectively. The maximum efficiency of Cr(VI) removal using $C_{12}$ min Br-Mt and $C_{16}$ min Br-Mt can be reached at pH 2.0. This phenomenon could be because of the different species of Cr(VI) at different pH conditions. Fig. 8 depicted a schematic illustration for the proposed mechanism of Cr(VI) on OMts. When the pH value was between 2.0 and 6.0, the major species of Cr(VI) present in the system was $HCrO_4^-$, and there was a small quantity of $Cr_2O_7^{2-}$; the surface of the OMts was positively charged so that the negative ions $HCrO_4^-$ and $Cr_2O_7^{2-}$ were effectively adsorbed onto the OMts via electrostatic attractions. Additionally, on the basis of the XRD results, it was concluded that the bilayer formation occurred on the interlayer of Na-Mt. Thus, the negative ions $HCrO_4^-$ and $Cr_2O_7^{2-}$ had anion exchange with the counter anion ($Br^-$) of the ILIs and can be adsorbed into the OMts via electrostatic attractions. Taking $C_{12}$ min Br-Mt as an example, at lower pH conditions, the adsorption of Cr(VI) occurred mainly via salt formation [($C_{12}$min) $HCrO_4$ and ($C_{12}$min)$_2$ $Cr_2O_7$] and to some extent via anion exchange. In this second case, the counter anion ($Br^-$) of $C_{12}$ min Br was displaced by $HCrO_4^-$ or $Cr_2O_7^{2-}$ from the exchange sites to form Mt-($C_{12}$min)$^+$-$HCrO_4^-$ or Mt-($C_{12}$min)$_2$ $Cr_2O_7^{2-}$ [18,29]. When the pH value was increased from 6.7 to 11.0, the major species changed from $HCrO_4^-$ to $CrO_4^{2-}$, and the area occupied per Cr(VI) ion evidently increased on average; the surface of the OMts was negatively charged. This led to electrostatic repulsion of the negatively charged Cr(VI) species, and hence the values of R decreased. Thus, it was concluded that the electrostatic interaction was the most important mechanism for Cr(VI) using $C_{12}$ min Br-Mt and $C_{16}$ min Br-Mt,and so the other experiments were carried out at pH 2.0.

The experiments were conducted with an adsorbent dose of 2.0 CEC, 2.0 g·L$^{-1}$, an initial concentration of 50 mg·L$^{-1}$, contact time of 4.0 h, and pH of 2.0 at room temperature. Fig. 9 shows the effects of contact time on the efficiency of Cr(VI) removal using $C_{12}$ min Br-Mt and $C_{16}$ min Br-Mt. The value of R increased rapidly to 87.86 % and 98.24% at 2.0 h for $C_{12}$ min Br-Mt and $C_{16}$ min Br-Mt, respectively, and showed no subsequent change within 2.0–4.0 h. Therefore, the adsorption time was fixed at 2.0 h in all of the adsorption experiments to ensure that the adsorption reached equilibrium.

### *3.3. Kinetics studies*

Pseudo-first order and pseudo-second order kinetics models were considered in this study. On the basis of

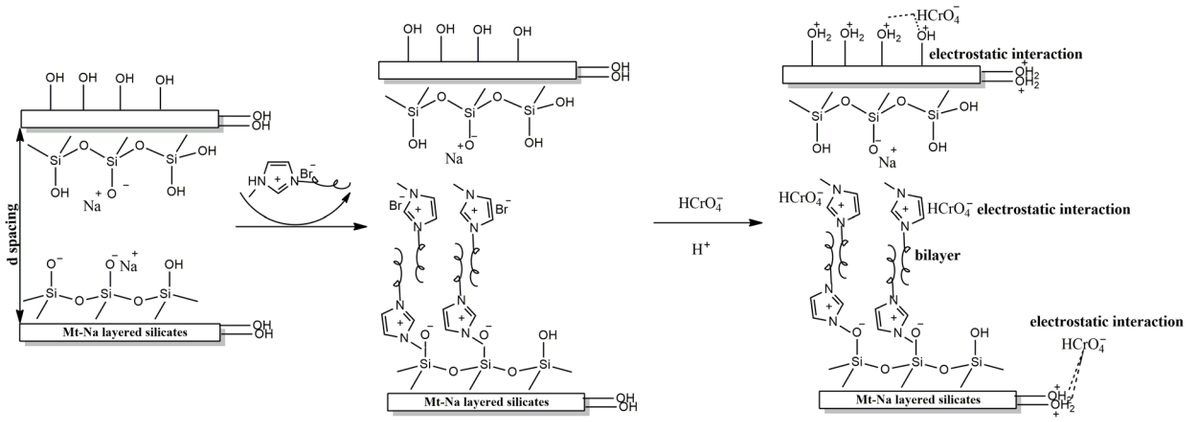


Fig. 8. Schematic illustration of the suggested mechanism for Cr(VI) on OMts.

the adsorption equilibrium capacity, these models can be expressed using Eqs. (3) and (4), respectively [31].

$$\ln(q_e - q_t) = k_1 t + \ln q_e \tag{3}$$

$$\frac{t}{q_t} = \frac{1}{q_e} t + \frac{1}{k_2 q_e^2} \tag{4}$$

where $q_e$ (mg·g$^{-1}$) and $q_t$ (mg·g$^{-1}$) represent the adsorption amount of Cr (VI) on OMts at equilibrium and at various time, respectively. $k_1$ (h$^{-1}$) is the pseudo-first order rate constant, $t$ (h) is the contact time, and $k_2$ (g·mg$^{-1}$·h$^{-1}$) is the pseudo-second order rate constant. The values of $k_1$ and $q_e$ for the pseudo-first order model and $k_2$ and $q_e$ for the pseudo-first order model can be determined from the linear plot of $\ln(q_e - q_t)$ vs. $t$ and the linear plot of $t/q_t$ vs. $t$, respectively; the results are given in Table 1. Both of the $R^2$ values are close to unity. The calculated values of $q_{e,cal}$ for $C_{12}$ min Br-Mt and $C_{16}$ min Br-Mt for the pseudo-first order model were 21.54 and 24.21 mg·g$^{-1}$, and these were consistent with the experimental values for $q_{e,exp}$. This demonstrated that the adsorption process of Cr (VI) by $C_{12}$ min Br-Mt and $C_{16}$ min Br-Mt followed the pseudo-second order reaction kinetics model.

Table 1
Kinetics parameters for Cr(VI) on $C_{12}$ min Br-Mt and $C_{16}$ min Br-Mt.

| Adsorbent | $q_{e,exp}$ | pseudo-firstorder | | | pseudo-secondorder | | |
|---|---|---|---|---|---|---|---|
| | | $q_{e,cal}$ | $k_1$ | $R^2$ | $q_{e,cal}$ | $k_2$ | $R^2$ |
| $C_{12}$minBr-Mt | 20.97 | 16.35 | 0.768 | 0.9434 | 21.54 | 1.451 | 0.9889 |
| $C_{16}$minBr-Mt | 24.56 | 20.24 | 1.352 | 0.9287 | 24.21 | 1.023 | 0.9988 |

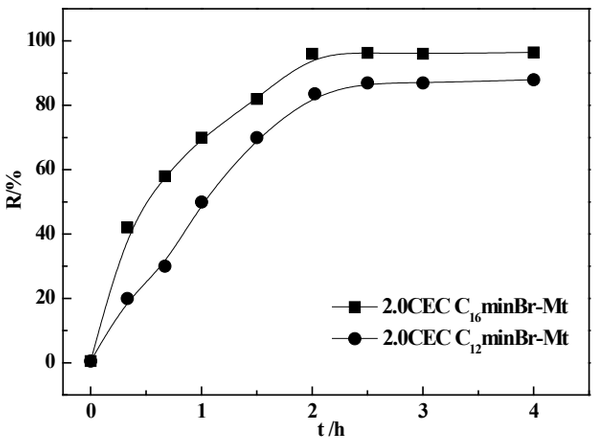


Fig. 9. Effects of contact time on the efficiency of Cr(VI) removal using $C_{12}$ min Br-Mt and $C_{16}$ min Br-Mt.

### 3.4. Adsorption isotherms

Both Langmuir and Freundlich adsorption isotherm models were used to describe the relationship between the amount of Cr (VI) adsorbed and its equilibrium concentration on $C_{12}$ min Br-Mt and $C_{16}$ min Br-Mt. The corresponding equations for the Langmuir and Freundlich models are as follows [31]:

$$\frac{C_e}{q_e} = \frac{1}{K_L q_{\max}} + \frac{C_e}{q_{\max}} \tag{5}$$

$$\ln q_e = \frac{1}{n} \ln C_e + \ln K_f \tag{6}$$

where $q_e$ (mg·g$^{-1}$) represents the adsorption amount of Cr (VI) on OMts at equilibrium. $C_e$ (mg·L$^{-1}$) is the equilibrium concentration in solution, and $q_{\max}$ (mg·g$^{-1}$) is the mono layer capacity of $C_{12}$ min Br-Mt or $C_{16}$ min Br-Mt. $K_L$(L·g$^{-1}$) is the Langmuir adsorption constant, which is related to the adsorption energy. $K_f$ (mg·g$^{-1}$) is the Freundlich constant, and $n$ is an indicator of the diversity of free energies associated with the sorption of the solute by multiple components of the heterogeneous sorbent.

The value of $n$ ranges from 1 to 10 and indicates that the adsorption process is favorable. The values of $q_{\max}$ and $K_L$ for the Langmuir isotherm model and $K_f$ and $n$ for the Freundlich isotherm model can be determined, respectively, from the linear plot of $C_e/q_e$ vs. $C_e$ and the linear plot of $ln\ q_e$ vs.

*ln* $C_e$. Fig. 10 showed the equilibrium adsorption isotherms of Cr(VI) on $C_{12}$ min Br-Mt and $C_{16}$ min Br-Mt at 20°C, and the adsorption isotherm constants were given in Table 2. As seen in Table 2, the $R^2$ values of the Langmuir isotherm (0.9912, 0.9976) are greater than those of the Freundlich isotherm (0.9534, 0.9287). This indicated that the Langmuir model was more suitable for describing the adsorption of Cr(VI) onto $C_{12}$ min Br-Mt and $C_{16}$ min Br-Mt than the Freundlich model.

### 3.5. Thermodynamics parameters

Thermodynamics studies of $C_{12}$ min Br-Mt and $C_{16}$ min Br-Mt can reveal the feasibility of and spontaneity of the adsorption process. The Gibbs free energy ($\Delta G^\theta$, kJ·mol$^{-1}$), the standard enthalpy ($\Delta H^\theta$, kJ·mol$^{-1}$), and the standard entropy ($\Delta S^\theta$, J·mol$^{-1}$) for the adsorption of Cr(VI) on $C_{12}$ min Br-Mt and $C_{16}$ min Br-Mt can be evaluated using the following equations [31]:

$$K = \frac{q_e}{C_e} \tag{7}$$

$$\ln K = \frac{\Delta S^\theta}{R} - \frac{\Delta H^\theta}{RT} \tag{8}$$

$$\Delta G^\theta = \Delta H^\theta - T\Delta S^\theta \tag{9}$$

where $q_e$ (mg·g$^{-1}$) represents the adsorption amount of Cr (VI) on OMts at equilibrium, and $C_e$ (mg·L$^{-1}$) is the equilibrium concentration of Cr (VI) in solution. $K$ is the equilibrium constant for the adsorption, $R$ (8.314 J·mol$^{-1}$·K$^{-1}$)is the gas constant, and $T$ (K$^{-1}$) is the absolute temperature of the solution. The values of $\Delta S^\theta$ and $\Delta H^\theta$ can be determined from the intercept and slope, respectively, of the linear plot of *ln K* vs. $1/T$; the values of $\Delta G^\theta$ were calculated at each temperature using Eq. (9). The experiments were done with an adsorbent dose of 2.0 CEC, 2.0 g·L$^{-1}$, an initial concentration of 50 mg·L$^{-1}$, contact time of 2.0 h, and pH of 2.0 at three temperatures (20, 30, and 40°C). The calculated thermodynamics parameters were shown in Table 3. Then negative values of $\Delta H^\theta$ indicated that the adsorption processes of Cr(VI) by $C_{12}$ min Br-Mt and $C_{16}$ min Br-Mt were exothermic. The negative values of $\Delta S^\theta$ indicated that the molecules of Cr(VI) changed from three-dimensional in solution to two-dimensional on the flat surfaces of OMts in the adsorption process, and then the randomness decreased [33]. The negative values of $\Delta G^\theta$ indicated that the adsorption process of Cr(VI) was spontaneous and the thermodynamically favorable process at the temperature of the experiment. At the same temperature, $\Delta G^\theta$ became more negative for $C_{16}$ min Br-Mt, indicating that $C_{16}$ min Br-Mt had stronger affinity for the negatively charged Cr(VI). Hence, the values of $\Delta G^\theta$ were in the range of 0 and –20 kJ·mol$^{-1}$, indicating that the adsorption process was ascribed to physisorption.

### 3.6. Comparison of Cr(VI) removal with various adsorbents

The significant effect of $C_{12}$ min Br-Mt and $C_{16}$ min Br-Mt on adsorption of Cr(VI) can be better explained by comparing them with other modified clays reported in the literature, as shown in Table 4. From Table 4, the $q_e$ of hexadecyltrimethyl ammonium-modified Mt (HDTMA-Mt), dodecylamine-modified Mt, dodecyltrimethylammonium chloride-modified Mt (DTAC-Mt) was 10.18, 23.69 and 10.44 mg·g$^{-1}$, respectively [17–19]. The $q_e$ of Mt modified with both cetyltrimethyl ammonium bromide and hydroxyaluminum (CTAB-OH-Al-Mt) was 11.97 mg·g$^{-1}$ [20]. For octadecyltrimethyl ammonium chloride modified bentonite (OTMAC-Bent) and organic-inorganic pillared bentonite (OTMAC-OH-Al-Bent), the $q_e$ was 12.40 and 19.75 mg·g$^{-1}$ respectively [17–19]. Obviously, $C_{12}$ min Br-Mt and $C_{16}$ min Br-Mt had a very high affinity for Cr(VI) compared to other modified clays. This provides strong evidence of the potential application of ILIs-modified Na-Mt for Cr(VI) and other anionic contaminants removal in wastewater.

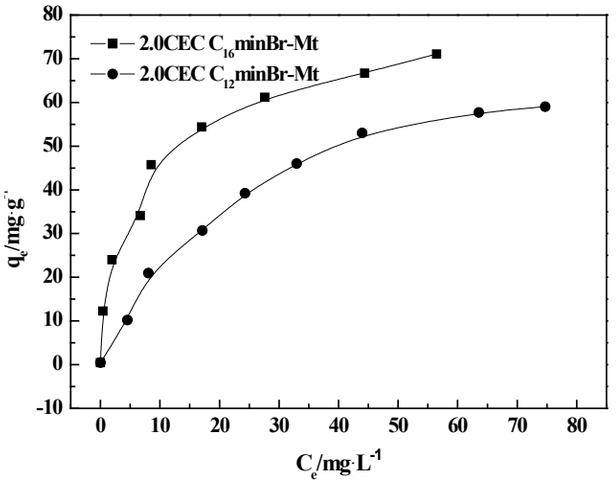


Fig. 10. Equilibrium adsorption isotherms of Cr(VI) on $C_{12}$ min Br-Mt and $C_{16}$ min Br-Mt at 20°C.

Table 2
Adsorption isotherm constants for adsorption of Cr(VI) on $C_{12}$ min Br-Mt and $C_{16}$ min Br-Mt at 20°C

| Adsorbent | Langmuir isotherm | | | Freundlich isotherm | | |
|---|---|---|---|---|---|---|
| | $q_{max}$ | $K_L$ | $R^2$ | $K_f$ | $1/n$ | $R^2$ |
| $C_{12}$minBr-Mt | 62.51 | 0.169 | 0.9912 | 2.681 | 0.582 | 0.9534 |
| $C_{16}$minBr-Mt | 70.42 | 0.891 | 0.9976 | 4.205 | 0.541 | 0.9287 |

Table 3
Thermodynamic parameters of Cr(VI) adsorption on $C_{12}$ min Br-Mt and $C_{16}$ min Br-Mt

| Adsorbents | $\Delta G^\theta$ | | | $\Delta S^\theta$ | $\Delta H^\theta$ |
|---|---|---|---|---|---|
| | T=293k | T=303k | T=313k | | |
| $C_{12}$minBr-Mt | –16.11 | –15.53 | –14.94 | –58.43 | –33.23 |
| $C_{16}$minBr-Mt | –19.25 | –18.19 | –17.13 | –106.15 | –50.35 |

Table 4
Comparison of adsorption capacities of $C_{12}$ min Br-Mt and $C_{16}$ min Br-Mt with various adsorbents

| Adsorbents | Adsorption capacity $q_e$ (mg·g$^{-1}$) | References |
|---|---|---|
| $C_{12}$ min Br-Mt | 20.97 | This work |
| $C_{16}$ min Br-Mt | 24.56 | This work |
| HDTMA-Mt | 10.18 | [17] |
| Dodecylamine- Mt | 23.69 | [18] |
| DTAC-Mt | 10.44 | [19] |
| CTAB-OH-Al-Mt | 11.97 | [20] |
| OTMAC-Bent | 12.40 | [33] |
| OTMAC-OH-Al-Bent | 19.75 | [33] |
| Na-Mt | 3.63 | [17] |

## 4. Conclusions

In this study, Na-Mt was modified using the ionic liquid-type cationic imidazolium surfactants $C_{12}$ mim Br and $C_{16}$ mim Br. FTIR, XRD, TG, and SEM results indicated that $C_{12}$ mim Br and $C_{16}$ mim Br were successfully inserted into the silicate layer, and the interlayer spacing and arrangement of the intercalary surfactants were related to the loading level and the length of the alkyl chain of the surfactants. According to the adsorption experiments, the adsorption of Cr(VI) on $C_{12}$ min Br-Mt and $C_{16}$ min Br-Mt was associated with the loading level of the surfactants, the contact time, and pH. The optimal conditions for the adsorption of 50 mg·L$^{-1}$ of Cr(VI) onto $C_{12}$ min Br-Mt and $C_{16}$ min Br-Mt were as follows: loading level of the surfactants was 2.0 CEC of Na-Mt, contact time was 2.0 h, and pH was 2.0. The removal efficiency of Cr(VI) on $C_{12}$ min Br-Mt and $C_{16}$ min Br-Mt increased to 83.88 % and 98.24%, respectively. For the same experimental conditions, $C_{16}$ mim Br-Mt had a stronger affinity for the negatively charged Cr(VI) because of electrostatic interactions. The adsorption kinetics were best described using a pseudo-second order kinetics model. The equilibrium adsorption data was analyzed using two isotherm models, and the adsorption isotherm was in good agreement with the Langmuir model. Using this model, the maximum adsorption capacities were 20.97 mg·g$^{-1}$ and 24.56 mg·g$^{-1}$ for $C_{12}$ mim Br-Mt and $C_{16}$ mim Br-Mt, respectively. The thermodynamics parameters showed that the adsorption was an exothermic, spontaneous physisorption process.

## Acknowledgment

This work was supported by the Chinese Ministry of Education through a National Undergraduate Training Programs for Innovation and Entrepreneurship 201610122004, the Natural Science Foundation of Shanxi Province 201701D121034, the Fund for Shanxi Key Subjects Construction, and Support Plan for Innovative Research Team of Changzhi University.

## References

[1] P.S. Keng, S.L. Lee, S.T. Ha, Y.T. Hung, S.T. Ong, Removal of hazardous heavy metals from aqueous environment by low-cost adsorption materials, Environ. Chem. Lett., 12 (2014) 15–25.
[2] A. Sarı, G. Sahinoglu, M. Tuzen, Antimony (III) adsorption from aqueous solution using raw perlite and Mn-modified perlite: equilibrium, thermodynamic, and kinetic studies, Ind. Eng. Chem. Res., 51 (2012) 6877–6886.
[3] M.H. Dehghani, D. Sanaei, I. Ali, A. Bhatnagar, Removal of chromium (VI) from aqueous solution using treated waste newspaper as a low-cost adsorbent: kinetic modeling and isotherm studies, J. Mol. Liq., 215 (2016) 671–679.
[4] Q. Jinghong, D. Shihua, W. Haibo, C. Xu, D. Zongliang, Adsorption performance of low-cost gelatin-montmorillonite nano composite for Cr( III ) ions, RSC Adv., 5 (2015) 58284–58291.
[5] X. Xuebing, C. Po-Hsiang, L. Guocheng, J. Wei-Teh, J. Jiin-Shuh, L. Libing, L. Zhaohui, Ionic-liquid-crafted zeolite for the removal of anionic dye methyl orange, J. Taiwan Inst. Chem. E., 59 (2016) 237–243.
[6] R. Huang, B. Yang, Q. Liu, Y. Liu, Simultaneous adsorption of aniline and Cr(VI) ion by activated carbon/chitosan composite, J. Appl. Polym. Sci., 131 (2014) 1001–1007.
[7] D. Park, Y.S. Yun, J.Y. Kim, J.M. Park, How to study Cr (VI) biosorption: Use of fermentation waste for detoxifying Cr (VI) in aqueous solution, Chem. Eng. J., 136 (2008) 173–179.
[8] D. Petruzzelli, R. Passino, G. Tiravanti, Ion exchange process for chromium removal and recovery from tannery wastes, Water Sci. Technol., 36 (1995) 197–207.
[9] S. Rengaraj, K.H. Yeon, S.H. Moon, Removal of chromium from water and wastewater by ion exchange resins, J. Hazard. Mater., 87 (2001) 273–287.
[10] C.A. Kozlowski, W. Walkowiak, Removal of chromium (VI) from aqueous solutions by polymer inclusion membranes, Water Res., 36 (2002) 4870–4876.
[11] F. Akbal, S. Camcı, Copper, chromium and nickel removal from metal plating wastewater by electro coagulation, Desalination, 269 (2011) 214–222.
[12] W. Yaoguang, H. Lihua, Z. Guangya, Y. Tao, Y. Liangguo, W. Qin, D. Bin, Removal of Pb(II) and methylene blue from aqueous solution by magnetic hydroxyapatite-immobilized oxidized multi-walled carbon nano tubes, J. Colloid Interface Sci., 494 (2017) 380–388.
[13] L. Wuhui, H. Tsuyoshi, S. Keiko, Optimization of hexadecylpyridinium-modified montmorillonite for removal of perchlorate based on adsorption mechanisms, Appl. Surf. Sci., 123 (2016) 29–36.
[14] K.U. Mohammad, A review on the adsorption of heavy metals by clay minerals, with special focus on the past decade, Chem. Eng. J., 308 (2017) 438–462.
[15] S.A. Boyd, G.Y. Sheng, B.J. Teppen, C.T. Johnston, Mechanisms for the adsorption of substituted nitrobenzenes by smectite clays, Environ. Sci. Technol., 35 (2001) 4227–4234.
[16] W.F. Jaynes, S.A. Boyd, Hydrophobicity of siloxane surfaces in smectites as revealed by aromatic hydrocarbon adsorption from water, Clays Clay Miner., 39 (1991) 428–436.
[17] S.T. Akar, Y. Yetimoglu, T. Gedikbey, Removal of chromium (VI) ions from aqueous solutions by using Turkish montmorillonite clay: effect of activation and modification, Desalination, 244 (2009) 97–108.
[18] A.S.K. Kumar, R. Ramachandran, S. Kalidhasan, V. Rajesh, N. Rajesh, Potential application of dodecylamine modified sodium montmorillonite as an effective adsorbent for hexavalent chromium, Chem. Eng. J., 211–212 (2012) 396–405.
[19] W. Guifang, H. Yuyan, S. Xin, S. Komarneni, M. Shaojian, W. Yujue, Cr(VI) adsorption by montmorillonite nano composites, Appl. Clay Sci., 125 (2016) 111–118.
[20] H. Bingjie, L. Hanjin, Adsorption of hexavalent chromium onto montmorillonite modified with hydroxyaluminum and cetyltrimethyl ammonium bromide, Appl. Surf. Sci., 257 (2010) 769–775.

[21] B. Avinash, M. Takeshi, S. Sukhprit, S. Kenichi, S. Hideki, A. Masahiko, Structural diversity, physico chemical properties and application of imidazolium surfactants: Recent advances, Adv. Colloid Interface Sci., 231 (2016) 36–58.
[22] R. Sadeghi, R. Golabiazar, Study of salt effects on the aggregation behavior of ionic liquid1-dodecyl-3-methylimidazolium bromide in aqueous solution, J. Mol. Liq., 197 (2014) 176–183.
[23] A. Cognigni, P. Gaertner, R. Zirbs, H. Peterlik, K. Prochazka, C. Schröder, K. Bica, Surface-active ionic liquids in micellar catalysis: Impact of anion selection on reaction rates in nucleophilic substitutions, Phys. Chem. Chem. Phys., 18 (2016) 13375–13384.
[24] S.M. Urahata, M.C.C. Ribeiro, Structure of ionic liquids of 1-alkyl-3-methyl-imidazolium cations: A systematic computer simulation study, J. Chem. Phys., 120 (2004) 1855–1863.
[25] G. Zheng, G. Manglai, L. Zhongxin, L. Laifu, Y. Yage, L. Yuening, Bis-pyridinium dibromides modified organo-bentonite for the removal of aniline from wastewater: a positive role of polar interaction, Appl. Clay Sci., 29 (2014) 107–115.
[26] C. Daimei, C. Jian, L. Xinlong, J. Haipeng, X. Zhiguo, Characterization of anion-cationic surfactants modified montmorillonite and its application for the removal of methyl orange, Chem. Eng. J., 171 (2011) 1150–1158.
[27] B. Makhoukhi, D. Villemin, M.A. Didi, Preparation, characterization and thermal stability of bentonite modified with bis-imidazolium salts, Mater. Chem. Phys., 138 (2013) 199–203.
[28] I.A. Lawal, B. Moodley, Synthesis, characterisation and application of imidazolium based ionic liquid modified montmorillonite sorbents for the removal of amaranth dye, RSC Adv., 5 (2015) 61913–61924.
[29] R. Guégan, M. Giovanela, F. Warmont, M. Motelica-Heino, Non-ionic organoclay: A 'Swiss Army knife' for the adsorption of organic micro-pollutants, J. Colloid Interface Sci., 437 (2015) 71–79.
[30] Z. Li, W.T. Jiang, P.H. Chang, G. Lv, S. Xu, Modification of a Ca-montmorill- onite with ionic liquids and its application for chromate removal, J. Hazard. Mater., 270 (2014)169–175.
[31] G. Uyar, H. Kaygusuz, F.B. Erim, Methylene blue removal by alginate-clay quasi-cryogel beads, React. Funct. Polym., 106 (2016) 1–7.
[32] Y.Q. Liang, H. Li, A comparison of trimeric surfactant intercalated montmorillonite with its gemini modified one: characterization and application in methyl orange removal, J. Mol. Liq., 227 (2017) 139–146.
[33] Z. Sen, Y. Jian, X. Xiaodong, Y. Liangguo, W. Qin, D. Bin, Adsorptive removal of Cr(VI) from aqueous solution onto different kinds of modified bentonites, Environ. Prog. Sustain., 34 (2014) 39–46.